

# Relativistic Hartree-Bogoliubov description of ground-state properties of Ni and Sn isotopes

G.A. Lalazissis<sup>1</sup>, D. Vretenar<sup>2</sup>, and P. Ring<sup>1</sup>

<sup>1</sup> *Physik-Department der Technischen Universität München, Garching, Germany*

<sup>2</sup> *Physics Department, Faculty of Science, University of Zagreb, Croatia*

(May 14, 2017)

## Abstract

The Relativistic Hartree Bogoliubov (RHB) theory is applied in the description of ground-state properties of Ni and Sn isotopes. The NL3 parameter set is used for the effective mean-field Lagrangian, and pairing correlations are described by the pairing part of the finite range Gogny interaction D1S. Fully self-consistent RHB solutions are calculated for the Ni ( $28 \leq N \leq 50$ ) and Sn ( $50 \leq N \leq 82$ ) isotopes. Binding energies, neutron separation energies, and proton and neutron *rms* radii are compared with experimental data. The model predicts a reduction of the spin-orbit potential with the increase of the number of neutrons. The resulting energy splittings between spin-orbit partners are discussed, as well as pairing properties calculated with the finite range effective interaction in the *pp* channel.

PACS numbers: 21.10.D, 21.10.F, 21.60.J, 21.30, 27.50, 27.60

## I. INTRODUCTION AND OUTLINE OF THE MODEL

Relativistic models of nuclear structure provide a consistent framework in which the nuclear many-body system is described in terms of interacting baryons and mesons. Detailed properties of finite nuclei along the  $\beta$ -stability line have been very successfully described in the framework of relativistic mean field models (for a recent review see Ref. [1]). In addition to the single-nucleon mean-field, pairing correlations have to be taken into account for a quantitative description of ground-state properties of open-shell nuclei. For nuclei close to the  $\beta$ -stability line, pairing has been included in the relativistic mean-field model in the form of a simple BCS approximation [2], with monopole pairing force adjusted to the experimental odd-even mass differences. Pairing correlations are also crucial for the description of deformations in heavy nuclei. However, as we move away from the valley of  $\beta$ -stable nuclei, the ground-state properties calculated within the BCS approximation become unreliable. In particular properties that crucially depend on the spatial extensions of nucleon densities, as for example nuclear radii. The reason is that the BCS scheme does

not provide a correct description of the scattering of nucleonic pairs from bound states to the positive energy particle continuum [3,4], and it leads to unbound systems. The solution, of course, is a unified description of mean-field and pairing correlations, as for example in the framework of the Hartree-Fock-Bogoliubov (HFB) theory. Within a non-relativistic approach to the nuclear many-body problem, HFB theory has a long and successful history of applications. In particular, HFB theory in coordinate space [3] has been used to describe properties of exotic nuclei with extreme isospin values, both on the neutron rich side [4], and proton drip-line nuclei [5].

The relativistic extension of the HFB theory was originally derived by Kucharek and Ring [6]. Starting from the Lagrangian of quantum hadrodynamics, they have been able to show that the pairing correlations result from the one-meson exchange ( $\sigma$ -,  $\omega$ - and  $\rho$ -mesons). The Relativistic Hartree-Bogoliubov (RHB) model developed in Ref. [6] is based on the Hartree approximation for the self-consistent mean field. However, if for the one-meson exchange pairing interaction in RHB one uses the coupling constants from standard parameter sets of the RMF model, the resulting pairing correlations are much too strong. The repulsion produced by the exchange of vector mesons at short distances results in a pairing gap at the Fermi surface that is by a factor three too large. On the other hand, it has been argued in many applications of the Hartree-Fock-Bogoliubov theory that there is no real reason for using the same effective forces in both the particle-hole and particle-particle channel. In a first-order approximation, the effective interaction contained in the mean-field  $\hat{\Gamma}$  is a  $G$ -matrix, the sum over all ladder diagrams. The effective force in the  $pp$  channel, i.e. in the pairing potential  $\hat{\Delta}$ , should be the  $K$  matrix, the sum of all diagrams irreducible in  $pp$ -direction. However, very little is known about this matrix in the relativistic framework and only phenomenological effective forces have been used in the  $pp$  channel of RHB. In the RHB calculations of Ref. [7] pairing correlations have been described by a two-body force of finite range of Gogny type [8],

$$V^{pp}(1,2) = \sum_{i=1,2} e^{-((\mathbf{r}_1-\mathbf{r}_2)/\mu_i)^2} (W_i + B_i P^\sigma - H_i P^\tau - M_i P^\sigma P^\tau), \quad (1)$$

with the parameters  $\mu_i$ ,  $W_i$ ,  $B_i$ ,  $H_i$  and  $M_i$  ( $i = 1, 2$ ). For the D1S [8] parameter set of the interaction the model was applied in the study of several isotope chains of spherical Pb, Sn and Zr nuclei. The pairing interaction is a sum of two Gaussians with finite range and properly chosen spin and isospin dependence. The Gogny force has been very carefully adjusted to the pairing properties of finite nuclei all over the periodic table. Its basic advantage is the finite range, which automatically guarantees a proper cut-off in momentum space. In Refs. [9,10] we have used RHB in coordinate space with the D1S Gogny interaction to study properties of light nuclear systems (C, N, O, F, Ne, Na, Mg) with large neutron excess. Self-consistent solutions were calculated for the ground-states of a number of neutron-rich nuclei. Predictions were obtained for the location of the neutron drip-line, reduction of the spin-orbit interaction, *rms* radii, changes of surface properties, formation of neutron skin and neutron halo. The effective interactions in the  $pp$  channel of the HFB theory were recently discussed in Ref. [4]. In particular, the role of finite range and the importance of density dependence were analyzed. Finite range forces have the obvious advantage of the automatic cut-off of high momentum components. On the other hand computations with zero-range forces are much simpler, although an artificial energy cut-off has to be included.

The density dependence of interactions in the pairing channel influences the spatial distributions of pairing densities and fields. By using interactions without density dependence, strong pairing fields are produced in the volume of the nucleus. There is experimental evidence that pairing is a surface effect, and by including a density dependent component the pairing field can be made surface peaked. A fully self-consistent RHB model in coordinate space, with a density dependent interaction of zero-range (delta force), has been used to describe the two-neutron halo in  $^{11}\text{Li}$  [11].

$$V(\mathbf{r}_1, \mathbf{r}_2) = V_0 \delta(\mathbf{r}_1 - \mathbf{r}_2) \frac{1}{4} (1 - \vec{\sigma}_1 \cdot \vec{\sigma}_2) \left[ 1 - \frac{\rho(r)}{\rho_0} \right] \quad (2)$$

In going away from the valley of  $\beta$ -stable nuclei, the main problem of nuclear structure models becomes the extrapolation of effective forces to nuclei with extreme isospin values. We have already applied RHB with the Gogny force in the pairing channel to light neutron-rich nuclei. However, many of these nuclei are still not accessible in experiments and therefore many of our results could not be compared with empirical data. In order to make predictions for medium-heavy nuclei at the neutron drip-line, we have to test available effective interactions in detailed calculations of properties of neutron rich nuclei for which a comparison with experimental data is possible. In the present article we consider two sets of isotopes: Ni ( $28 \leq N \leq 50$ ) and Sn ( $50 \leq N \leq 82$ ). Such an analysis will test the predictions of effective forces in both the  $ph$  and  $pp$  channel over two major neutron shells. In addition to the effects of the pairing interaction, we are particularly interested in the behavior of the spin-orbit term of the effective potential as function of the neutron number. For light neutron rich nuclei, in Ref. [12] we have shown that the magnitude of the spin-orbit potential is considerably reduced at the drip-line, resulting in much smaller energy splittings between spin-orbit partners. For the Ne isotopes this reduction was found to be around forty percent. Since it seems that at present only relativistic models include the correct isospin dependence of the spin-orbit term in the mean-field potential, it would be important to study in medium-heavy nuclei the predicted spacings of single-neutron levels close to the Fermi surface.

The details of the RHB model are given in Refs. [10,13]. A short outline of essential features follows. The ground state of a nucleus  $|\Phi\rangle$  is described as vacuum with respect to independent quasi-particle operators, which are defined by a unitary Bogoliubov transformation of the single-nucleon creation and annihilation operators. The generalized single-nucleon Hamiltonian contains two average potentials: the self-consistent mean-field  $\hat{\Gamma}$  which encloses all the long range  $ph$  correlations, and a pairing field  $\hat{\Delta}$  which sums up the  $pp$  correlations. The expectation value of the nuclear Hamiltonian  $\langle \Phi | \hat{H} | \Phi \rangle$  is a function of the hermitian density matrix  $\rho$ , and the antisymmetric pairing tensor  $\kappa$ . The variation of the energy functional with respect to  $\rho$  and  $\kappa$  produces the single quasi-particle Hartree-Fock-Bogoliubov equations [14]. The relativistic extension of the HFB theory was introduced in Ref. [6]. In the Hartree approximation for the self-consistent mean field, the Relativistic Hartree-Bogoliubov (RHB) equations read

$$\begin{pmatrix} \hat{h}_D - m - \lambda & \hat{\Delta} \\ -\hat{\Delta}^* & -\hat{h}_D + m + \lambda \end{pmatrix} \begin{pmatrix} U_k(\mathbf{r}) \\ V_k(\mathbf{r}) \end{pmatrix} = E_k \begin{pmatrix} U_k(\mathbf{r}) \\ V_k(\mathbf{r}) \end{pmatrix}. \quad (3)$$

where  $\hat{h}_D$  is the single-nucleon Dirac Hamiltonian (4) and  $m$  is the nucleon mass. The chemical potential  $\lambda$  has to be determined by the particle number subsidiary condition, in order that the expectation value of the particle number operator in the ground state equals the number of nucleons. The column vectors denote the quasi-particle wave functions, and  $E_k$  are the quasi-particle energies. The Dirac Hamiltonian

$$\hat{h}_D = -i\boldsymbol{\alpha} \cdot \boldsymbol{\nabla} + \beta(m + g_\sigma \sigma) + g_\omega \omega^0 + g_\rho \tau_3 \rho_3^0 + e \frac{(1 - \tau_3)}{2} A^0 \quad (4)$$

contains the mean-field potentials of the isoscalar scalar  $\sigma$ -meson, the isoscalar vector  $\omega$ -meson and the isovector vector  $\rho$ -meson.  $A^0$  is the electrostatic potential. The RHB equations have to be solved self-consistently, with potentials determined in the mean-field approximation from solutions of Klein-Gordon equations

$$[-\Delta + m_\sigma^2] \sigma(\mathbf{r}) = -g_\sigma \rho_s(\mathbf{r}) - g_2 \sigma^2(\mathbf{r}) - g_3 \sigma^3(\mathbf{r}) \quad (5)$$

$$[-\Delta + m_\omega^2] \omega^0(\mathbf{r}) = -g_\omega \rho_v(\mathbf{r}) \quad (6)$$

$$[-\Delta + m_\rho^2] \rho^0(\mathbf{r}) = -g_\rho \rho_3(\mathbf{r}) \quad (7)$$

$$-\Delta A^0(\mathbf{r}) = e \rho_p(\mathbf{r}). \quad (8)$$

for the sigma meson, omega meson, rho meson and photon field, respectively. The spatial components  $\boldsymbol{\omega}$ ,  $\boldsymbol{\rho}_3$  and  $\mathbf{A}$  vanish due to time reversal symmetry. The equation for the sigma meson contains the non-linear  $\sigma$  self-interaction terms [15]. Because of charge conservation, only the 3-component of the isovector rho meson contributes. The source terms in equations (5) to (8) are sums of bilinear products of baryon amplitudes

$$\rho_s(\mathbf{r}) = \sum_{E_k > 0} V_k^\dagger(\mathbf{r}) \gamma^0 V_k(\mathbf{r}), \quad (9)$$

$$\rho_v(\mathbf{r}) = \sum_{E_k > 0} V_k^\dagger(\mathbf{r}) V_k(\mathbf{r}), \quad (10)$$

$$\rho_3(\mathbf{r}) = \sum_{E_k > 0} V_k^\dagger(\mathbf{r}) \tau_3 V_k(\mathbf{r}), \quad (11)$$

$$\rho_{em}(\mathbf{r}) = \sum_{E_k > 0} V_k^\dagger(\mathbf{r}) \frac{1 - \tau_3}{2} V_k(\mathbf{r}). \quad (12)$$

where the sums run over all positive energy states. The pairing field  $\hat{\Delta}$  in (3) is defined

$$\Delta_{ab}(\mathbf{r}, \mathbf{r}') = \frac{1}{2} \sum_{c,d} V_{abcd}(\mathbf{r}, \mathbf{r}') \kappa_{cd}(\mathbf{r}, \mathbf{r}'). \quad (13)$$

where  $a, b, c, d$  denote quantum numbers that specify the single-nucleon states.  $V_{abcd}(\mathbf{r}, \mathbf{r}')$  are matrix elements of a general two-body pairing interaction, and the pairing tensor is defined

$$\kappa_{cd}(\mathbf{r}, \mathbf{r}') = \sum_{E_k > 0} U_{ck}^*(\mathbf{r}) V_{dk}(\mathbf{r}'). \quad (14)$$

The eigensolutions of Eq. (3) form a set of orthogonal and normalized single quasi-particle states. The corresponding eigenvalues are the single quasi-particle energies. The self-consistent iteration procedure is performed in the basis of quasi-particle states. The resulting quasi-particle eigenspectrum is then transformed into the canonical basis of single-particle states, in which the RHB ground-state takes the BCS form. The transformation determines the energies and occupation probabilities of the canonical states.

For nuclear systems with spherical symmetry the fields  $\sigma(r)$ ,  $\omega^0(r)$ ,  $\rho^0(r)$ , and  $A^0(r)$  depend only on the radial coordinate  $r$ . The nucleon spinors  $U_k$  ( $V_k$ ) in (3) are characterized by the angular momentum  $j$ , its  $z$ -projection  $m$ , parity  $\pi$  and the isospin  $t_3 = \pm\frac{1}{2}$  for neutron and proton. The two Dirac spinors  $U_k(\mathbf{r})$  and  $V_k(\mathbf{r})$  are defined

$$U_k(V_k)(\mathbf{r}, s, t_3) = \begin{pmatrix} g_{U(V)}(r)\Omega_{j,l,m}(\theta, \varphi, s) \\ if_{U(V)}(r)\Omega_{j,\bar{l},m}(\theta, \varphi, s) \end{pmatrix} \chi_\tau(t_3). \quad (15)$$

$g(r)$  and  $f(r)$  are radial amplitudes,  $\chi_\tau$  is the isospin function, and  $\Omega_{jlm}$  is the tensor product of the orbital and spin functions

$$\Omega_{j,l,m}(\theta, \varphi, s) = \sum_{m_s, m_l} \frac{1}{2} \langle \frac{1}{2} m_s l m_l | j m \rangle \chi_{\frac{1}{2} m_s} Y_{lm_l}(\theta, \varphi). \quad (16)$$

The two-component functions

$$\Phi_U(r) := \begin{pmatrix} g_U(r) \\ if_U(r) \end{pmatrix} \quad \text{and} \quad \Phi_V(r) := \begin{pmatrix} g_V(r) \\ if_V(r) \end{pmatrix}, \quad (17)$$

are solutions of the Dirac-Hartree-Bogoliubov equations

$$\begin{aligned} (\hat{h}_D(r) - m - \lambda)\Phi_U(r) + \int_0^\infty dr' r'^2 \Delta(r, r') \Phi_V(r') &= E\Phi_U(r) \\ (-\hat{h}_D(r) + m + \lambda)\Phi_V(r) + \int_0^\infty dr' r'^2 \Delta(r, r') \Phi_U(r') &= E\Phi_V(r) \end{aligned} \quad (18)$$

The self-consistent solution of the Dirac-Hartree-Bogoliubov integro-differential eigenvalue equations and Klein-Gordon equations for the meson fields determines the nuclear ground state. In Refs. [9,10,12,13] we have used Finite Element Methods in the coordinate space discretization of the coupled system of equations. In order to correctly describe structure phenomena in exotic nuclei with extreme isospin values, as for example regions of neutron halos with very diffuse neutron densities, the RHB equations have to be solved in coordinate space. However, for the spherical nuclear systems that we consider in the present article this is not necessary [3]. As it was done in Ref. [7], the Dirac-Hartree-Bogoliubov equations and the equations for the meson fields are solved by expanding the nucleon spinors  $U_k(\mathbf{r})$  and  $V_k(\mathbf{r})$ , and the meson fields in a basis of spherical harmonic oscillators for  $N = 20$  oscillator shells [2]. For odd-A isotopes we also include the blocking procedure [14] for neutron levels. Strictly speaking, for these nuclei also the assumption about currents is no longer valid, and in general one should include the fields  $\boldsymbol{\omega}$ ,  $\boldsymbol{\rho}_3$  and  $\mathbf{A}$ . However, the spatial components of the vector fields do not significantly contribute to the ground state properties investigated in the present work, and therefore they have not been included in our calculations.

## II. GROUND-STATES OF NI AND SN ISOTOPES

The details of ground-state properties of Ni ( $28 \leq N \leq 50$ ) and Sn ( $50 \leq N \leq 82$ ) isotopes will depend on the choice of the effective mean-field Lagrangian in the  $ph$  channel, as well as on the effective pairing interaction. Several parameter sets of the mean-field Lagrangian have been derived that provide a satisfactory description of nuclear properties along the  $\beta$ -stability line. In particular, NL1 [16], NL3 [17], and NL-SH [18]. The effective forces NL1 and NL-SH have been used in many analyses to calculate properties of nuclear matter and of finite nuclei, and have become standard parameterizations for relativistic mean-field calculations. The effective interaction NL1 was also used in the RHB+Gogny calculations of Ref. [7]. More recently the parameter set NL3 has been derived [17] by fitting ground state properties of a large number of spherical nuclei. Properties calculated with the NL3 effective interaction are found to be in very good agreement with experimental data for nuclei at and away from the line of  $\beta$ -stability. In Ref. [19] it has been shown that constrained RMF calculations with the NL3 effective force reproduce the excitation energies of superdeformed minima relative to the ground-state in  $^{194}\text{Hg}$  and  $^{194}\text{Pb}$ . In the same work the NL3 interaction was also used for calculations of binding energies and deformation parameters of rare-earth nuclei. We have used the NL3 parameter set in our study of light neutron-rich nuclei in Refs. [9,10,12]. For Ni and Sn the objective is to study how well does the NL3 effective force describe systems with very different number of neutrons, without going to nuclei with extreme isospin values. Only if it were shown that the isospin dependence of NL3 is correct, this interaction could be used to make reliable predictions about medium-heavy drip-line nuclei. This could be especially important for Ni, since there is hope that drip-line isotopes might become accessible in experiments. Pairing being essentially a non-relativistic effect, we use the Gogny interaction in the  $pp$  channel with the parameter set D1S [8]. Results obtained with this effective force might also indicate the path one should take in deriving a fully relativistic theory of pairing, consistent with the modern mean-field Lagrangians.

In Figs. 1 and 2 we display the one- and two-neutron separation energies

$$S_n(Z, N) = B_n(Z, N) - B_n(Z, N - 1) \quad (19)$$

$$S_{2n}(Z, N) = B_n(Z, N) - B_n(Z, N - 2) \quad (20)$$

for Ni ( $24 \leq N \leq 50$ ) and Sn ( $50 \leq N \leq 88$ ) isotopes, respectively. The values that correspond to the self-consistent RHB ground-states are compared with experimental data and extrapolated values from Ref. [20]. The theoretical values reproduce in detail the experimental separation energies. The model describes not only the empirical values within one major neutron shell, but it also reproduces the transitions between major shells. The results are excellent for the region beyond the shell closure at  $N = 82$  in Sn. The agreement with experimental data is somewhat worse for neutrons in the  $1f_{7/2}$  orbital in Ni isotopes, although the general trend is reproduced. However, these nuclei ( $24 \leq N \leq 28$ ) really belong to the proton-rich side and are not a primary objective of the present study. The total binding energies for Ni and Sn isotopes are compared with experimental values in Fig. 3. Except for the region around  $^{60}\text{Ni}$  and for  $^{100-102}\text{Sn}$ , the absolute differences between the calculated

and experimental masses are less than 2 MeV. For Ni the model predicts weaker binding for  $N \leq 40$ . Compared to experimental values, the theoretical binding energies are  $\approx 1$  MeV larger for neutrons in the  $1g_{9/2}$  orbital ( $40 \leq N \leq 50$ ). For Sn isotopes the results of model calculation in general display an overbinding. The differences are larger for  $^{100-102}\text{Sn}$ , but we expect that for these nuclei additional correlations should be taken into account in order to get a better agreement with experimental data. In particular, proton-neutron pairing could influence the masses in this region. Proton-neutron short-range correlations are not included in our model.

In Fig. 4 we show the self-consistent ground-state neutron densities for the Sn and Ni nuclei. The density profiles display shell effects in the bulk and a gradual increase of neutron radii. In the insert of Fig. 4 we include the corresponding values for the surface thickness and diffuseness parameter. The surface thickness  $t$  is defined to be the change in radius required to reduce  $\rho(r)/\rho_0$  from 0.9 to 0.1 ( $\rho_0$  is the maximal value of the neutron density; because of shell effects we could not use for  $\rho_0$  the density in the center of the nucleus). The diffuseness parameter  $\alpha$  is determined by fitting the neutron density profiles to the Fermi distribution

$$\rho(r) = \rho_0 \left( 1 + \exp\left(\frac{r - R_0}{\alpha}\right) \right)^{-1}, \quad (21)$$

where  $R_0$  is the half-density radius. By adding more units of isospin the value of the neutron surface thickness increases and the surface becomes more diffuse. The increase in  $t$  and  $\alpha$  is more uniform in Sn, and both parameters increase approximately forty percent from  $^{100}\text{Sn}$  to  $^{132}\text{Sn}$ . A somewhat smaller increase in the surface thickness is observed for Ni isotopes. The diffuseness parameter for Ni is essentially a step function:  $\alpha \approx 0.45$  fm for  $N < 40$  and  $\alpha \approx 0.50$  fm for neutrons in the  $1g_{9/2}$  orbital. We will show that the observed changes in surface properties result from the reduction of the spin-orbit term in the effective single-nucleon potential.

In Figs. 5 and 6 we display the neutron and proton *rms* radii for Ni and Sn isotopes, respectively. The calculated values are compared with experimental neutron radii from Ref. [21], and with data for proton radii from Ref. [22]. In the lowest panels we also compare the differences  $r_n - r_p$ . We find an excellent agreement between experimental data and values calculated with the NL3 effective force with the D1S Gogny interaction in the pairing channel. The model predicts a uniform increase of *rms* radii with the number of neutrons. The neutron skin  $r_n - r_p$  increases to approximately 0.4 fm at the closed shells  $N = 50$  for Ni, and  $N = 82$  for Sn.

In Ref. [12] we have shown that in the framework of the relativistic mean-field model the magnitude of the spin-orbit term in the effective single nucleon potential is greatly reduced for light neutron rich nuclei. With the increase of the number of neutrons the effective spin-orbit interaction becomes weaker and this results in a reduction of the energy splittings for spin-orbit partners. The reduction in the surface region was found to be as large as  $\approx 40\%$  for Ne isotopes at the drip-line. The spin-orbit potential originates from the addition of two large fields: the field of the vector mesons (short range repulsion), and the scalar field of the sigma meson (intermediate attraction). In the first order approximation, and assuming spherical symmetry, the spin orbit term can be written as

$$V_{s.o.} = \frac{1}{r} \frac{\partial}{\partial r} V_{ls}(r), \quad (22)$$

where  $V_{ls}$  is the spin-orbit potential [23]

$$V_{ls} = \frac{m}{m_{eff}}(V - S). \quad (23)$$

$V$  and  $S$  denote the repulsive vector and the attractive scalar potentials, respectively.  $m_{eff}$  is the effective mass

$$m_{eff} = m - \frac{1}{2}(V - S). \quad (24)$$

Using the vector and scalar potentials from the NL3 self-consistent ground-state solutions, we have computed from (22) - (24) the spin-orbit terms for the Ni and Sn isotopes. They are displayed in Figs. 7 and 8 as function of the radial distance from the center of the nucleus. The magnitude of the spin-orbit term  $V_{s.o.}$  decreases as we add more neutrons, i.e. more units of isospin. If we compare  $^{56}\text{Ni}$  with  $^{78}\text{Ni}$ , in Fig. 7, the reduction is  $\approx 35\%$  in the surface region. This implies a significant weakening of the spin-orbit interaction. The minimum of  $V_{s.o.}$  is also shifted outwards, and this reflects the larger spatial extension of the scalar and vector densities, which become very diffuse on the surface. The reduction of the spin-orbit term seems to be less pronounced in the Sn isotopes (Fig. 8), and this indicates that the weakening of the spin-orbit interaction might be not that important in heavy nuclei. The effect is reflected in the calculated spin-orbit splittings of the neutron levels in the canonical basis

$$\Delta E_{ls} = E_{n,l,j=l-1/2} - E_{n,l,j=l+1/2}, \quad (25)$$

In Fig. 9 we display the energy splittings of spin-orbit neutron partners for Ni and Sn, respectively. The calculated spacings are shown as function of the neutron number. We only include the spin-orbit doublets for which one of the partners is an intruder orbital in a major shell. These doublets display the largest energy splittings. We notice in Fig. 9 that the spacing between spin-orbit partners decreases with neutron number. The effect is stronger in Ni than in Sn, and quantitatively the observed decrease is consistent with the gradual weakening of the spin-orbit term shown in Figs. 7 and 8.

In order to illustrate the properties of the interaction in the  $pp$  channel, in Figs. 10 and 11 we plot the average values of the neutron canonical pairing gaps  $\Delta_{nlj}$  as functions of canonical single-particle energies. The gaps are displayed for canonical states that correspond to the self-consistent ground states of  $^{70}\text{Ni}$  and  $^{120}\text{Sn}$ , respectively.  $\Delta_{nlj}$  are the diagonal matrix elements of the pairing part of the RHB single-nucleon Hamiltonian in the canonical basis. Although not completely equivalent,  $\Delta_{nlj}$  corresponds to the pairing gap in BCS theory. A very detailed discussion of HFB equations in the canonical basis can be found in Ref. [4]. For  $^{120}\text{Sn}$  (Fig. 11) we essentially reproduce the results calculated in Ref. [4] with the Gogny HFB+D1S model. The calculated pairing gaps are almost identical, although there is a difference in the canonical single-neutron energies due to different effective forces used in the  $ph$  channel. While we employ the NL3 effective meson-exchange interaction in the  $ph$  channel, in the calculation of Ref. [4] the Gogny effective force has been used both in the  $ph$



and  $pp$  channel. The pairing gaps display a uniform decrease with single-neutron energies. This is related to the volume character of the Gogny interaction in the pairing channel. The values of the  $\Delta_{nlj}$  for the  $s_{1/2}$  orbitals are slightly larger, and the average value at the Fermi surface is around 1.5 MeV. It should be noted that for the HFB+SkP calculations of Ref. [4] the values of the pairing gaps are strongly peaked at the Fermi surface. In addition, we have calculated the average canonical pairing gaps for  $^{70}\text{Ni}$  (Fig. 10). As compared with  $^{120}\text{Sn}$ , the  $\Delta_{nlj}$  display a very similar behavior for deep-hole states (although for  $1s_{1/2}$  the pairing gap is considerably smaller), but they decrease more slowly for canonical states in the single-neutron continuum. At the Fermi surface the average values are between 1 and 1.5 MeV, somewhat smaller than in  $^{120}\text{Sn}$ .

Finally in Fig. 12 we compare the averages of the neutron pairing gaps for occupied canonical states

$$\langle \Delta_N \rangle = \frac{\sum_{nlj} \Delta_{nlj} v_{nlj}^2}{\sum_{nlj} v_{nlj}^2}, \quad (26)$$

where  $v_{nlj}^2$  are the occupation probabilities. The quantities  $\langle \Delta_N \rangle$  are plotted as functions of the neutron number for Ni and Sn isotopes. Solid lines correspond to even, and dashed lines to odd-neutron isotopes.  $\langle \Delta_N \rangle$  provides an excellent quantitative measure of pairing correlations. The quasi-parabolic functional dependence on the number of neutrons reflects the increase of pairing correlations toward the middle of a major shell. Both for Ni and Sn the values of  $\langle \Delta_N \rangle$  are above 2 MeV in the middle of the corresponding shells. As one would expect, the values for odd-neutron isotopes are somewhat lower. While in Sn the average pairing gaps do not provide any indication of additional shell effects, in Ni they very clearly indicate the shell subclosure at  $N = 40$ . It is also interesting to note that pairing correlations are stronger in the subshell  $28 \leq N \leq 40$ , than for neutrons in the  $1g_{9/2}$  orbital.

In conclusion, in the present work we have performed a detailed analysis of ground-state properties of Ni ( $28 \leq N \leq 50$ ) and Sn ( $50 \leq N \leq 82$ ) nuclei in the framework of the Relativistic Hartree Bogoliubov theory. The NL3 parameter set has been used for the effective mean-field Lagrangian in the  $ph$  channel, and pairing correlations have been described by the finite range Gogny interaction D1S. In a comparison with available experimental data, we have shown that the NL3 + Gogny D1S effective interaction provides an excellent description of binding energies, neutron separation energies, and proton and neutron  $rms$  radii. The results indicate that this choice of model parameters might also be valid for nuclei with more extreme isospin values, i.e. medium-heavy nuclei at the drip-lines. We have also discussed the predicted reduction of the effective spin-orbit potential with the increase of the number of neutrons, as well as the resulting energy splittings between spin-orbit partners and modifications of surface properties. Pairing properties calculated with the finite range effective interaction in the  $pp$  channel have been carefully analyzed. These results are particularly important since one of the main objectives of RHB theory should be a fully relativistic description of pairing correlations, consistent with modern mean-field Lagrangians.

## REFERENCES

- [1] P. Ring, *Progr. Part. Nucl. Phys.* **37**, 193 (1996).
- [2] Y.K. Gambhir, P. Ring, and A. Thimet, *Ann. Phys. (N.Y.)* **511**, 129 (1990).
- [3] J. Dobaczewski, H. Flocard, and J. Treiner, *Nucl. Phys.* **A422**, 103 (1984).
- [4] J. Dobaczewski, W. Nazarewicz, T. R. Werner, J. F. Berger, C. R. Chinn, and J. Dechargé, *Phys. Rev. C* **53**, 2809 (1996).
- [5] W. Nazarewicz, J. Dobaczewski, T. R. Werner, J. A. Maruhn, P.-G. Reinhard, K. Rutz, C. R. Chinn, A. S. Umar and M. R. Strayer, *Phys. Rev. C* **53**, 740 (1996).
- [6] H. Kucharek and P. Ring; *Z. Phys.* **A 339**, 23 (1991).
- [7] T. Gonzalez-Llarena, J.L. Egido, G.A. Lalazissis, and P. Ring, *Phys. Lett. B* **379**, 13 (1996).
- [8] J. F. Berger, M. Girod and D. Gogny, *Nucl. Phys.* **A428**, 32 (1984).
- [9] W. Pöschl, D. Vretenar, G.A. Lalazissis, and P. Ring, *Phys. Rev. Lett.* **79**, 3841 (1997).
- [10] G.A. Lalazissis, D. Vretenar, W. Pöschl, and P. Ring, *Nucl. Phys.* **AXXX**, (1998).
- [11] J. Meng and P. Ring, *Phys. Rev. Lett.* **77**, 3963 (1996).
- [12] G.A. Lalazissis, D. Vretenar, W. Pöschl, and P. Ring, *Phys. Lett. B* (1997).
- [13] W. Pöschl, D. Vretenar and P. Ring, *Comput. Phys. Commun.* **103**, 217 (1997).
- [14] P. Ring, and P. Schuck, "The Nuclear Many-Body Problem" (Springer-Verlag, Heidelberg 1980).
- [15] J. Boguta and A.R. Bodmer, *Nucl. Phys.* **A292**, 413 (1977).
- [16] P.G. Reinhard, M.Rufa, J. Maruhn, W. Greiner and J. Friedrich, *Z. Phys.* **A 323**, 13 (1986).
- [17] G.A. Lalazissis, J. König, and P. Ring, *Phys. Rev. C* **55**, 540 (1997).
- [18] M.M. Sharma, M.A. Nagarajan, and P. Ring; *Phys. Lett.* **B312**, 377 (1993).
- [19] G.A. Lalazissis and P. Ring, *Phys. Lett. B* **XXX**, (1998).
- [20] G. Audi and A. H. Wapstra, *Nucl. Phys.* **A595**, 409 (1995).
- [21] C.J. Batty, E. Friedman, H.J. Gils, and H. Rebel, *Adv. Nucl. Phys.* **19**, 1 (1989).
- [22] H. de Vries, C.W. de Jager, and C. de Vries, *At. Data Nucl. Data Tables* **36**, 495(1987).
- [23] W. Koepf and P. Ring, *Z. Phys.* **A339**, 81 (1991).

## FIGURES

FIG. 1. One and two-neutron separation energies for Ni isotopes calculated in the RHB model and compared with experimental data.

FIG. 2. Comparison between RHB model and experimental one and two-neutron separation energies for Sn isotopes.

FIG. 3. Differences between RHB model and experimental binding energies for Ni and Sn isotopes.

FIG. 4. Self-consistent RHB single-neutron density distributions for Sn ( $50 \leq N \leq 82$ ) and Ni ( $28 \leq N \leq 50$ ) nuclei, calculated with the NL3 effective interaction.

FIG. 5. Calculated neutron and proton *rms* radii for Ni isotopes compared with experimental data.

FIG. 6. Calculated and experimental neutron and proton *rms* radii for Sn isotopes.

FIG. 7. Radial dependence of the spin-orbit term of the potential in self-consistent solutions for the ground-states of Ni ( $28 \leq N \leq 50$ ) nuclei.

FIG. 8. Radial dependence of the spin-orbit term of the potential in self-consistent solutions for the ground-states of Sn ( $50 \leq N \leq 82$ ) nuclei.

FIG. 9. Energy splittings between spin-orbit partners for neutron levels in Ni and Sn isotopes, as functions of neutron number.

FIG. 10. Average values of the neutron canonical pairing gaps as functions of canonical single-particle energies for states that correspond to the self-consistent ground state of  $^{70}\text{Ni}$ . The NL3 parametrization has been used for the mean-field Lagrangian, and the parameter set D1S for the pairing interaction.

FIG. 11. Same as in the previous figure, but for the canonical states that correspond to the ground state of  $^{120}\text{Sn}$ .

FIG. 12. Average neutron pairing gaps  $\langle \Delta_N \rangle$  for the Ni and Sn isotopes, as functions of neutron number.

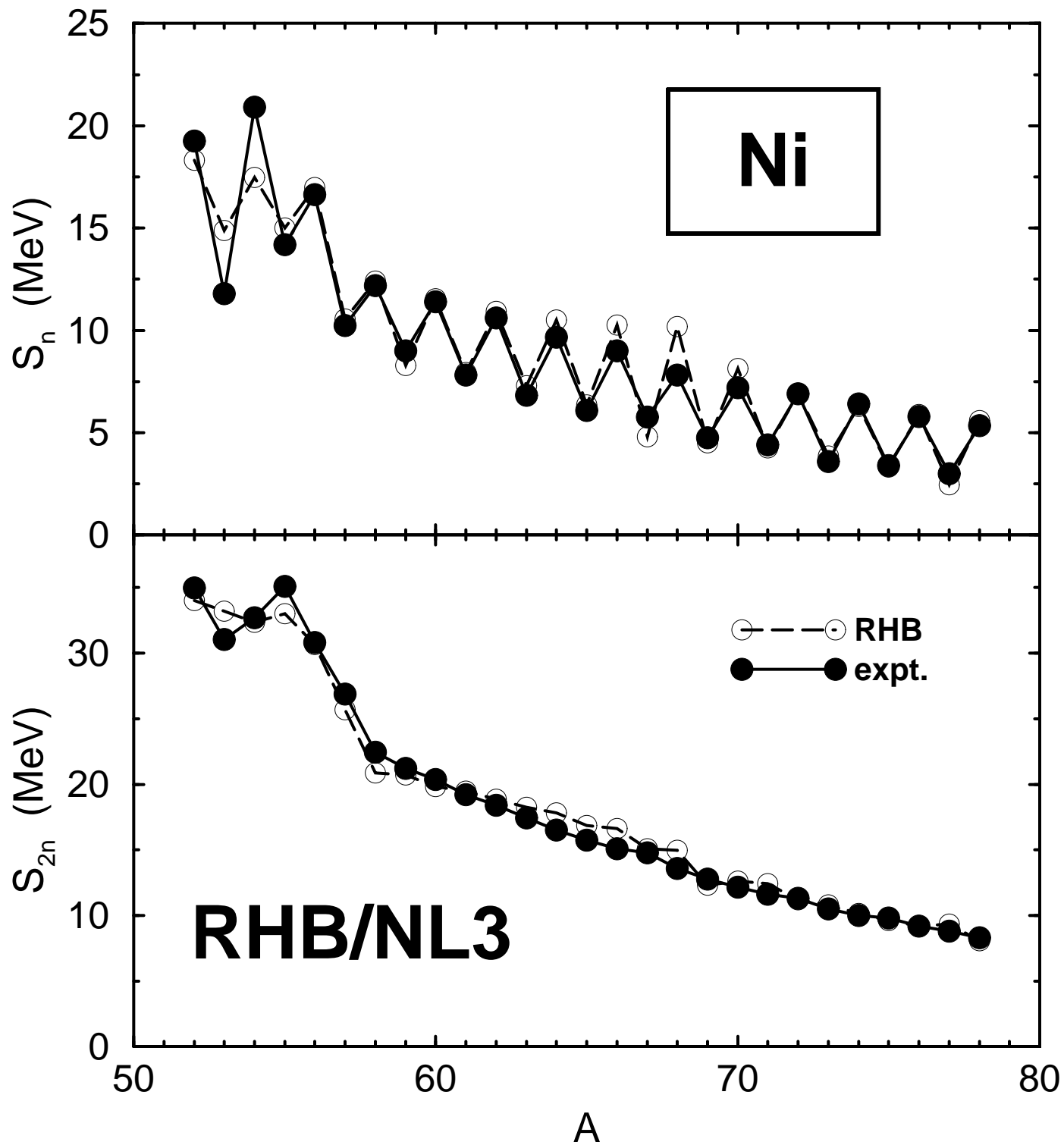


Fig. 1

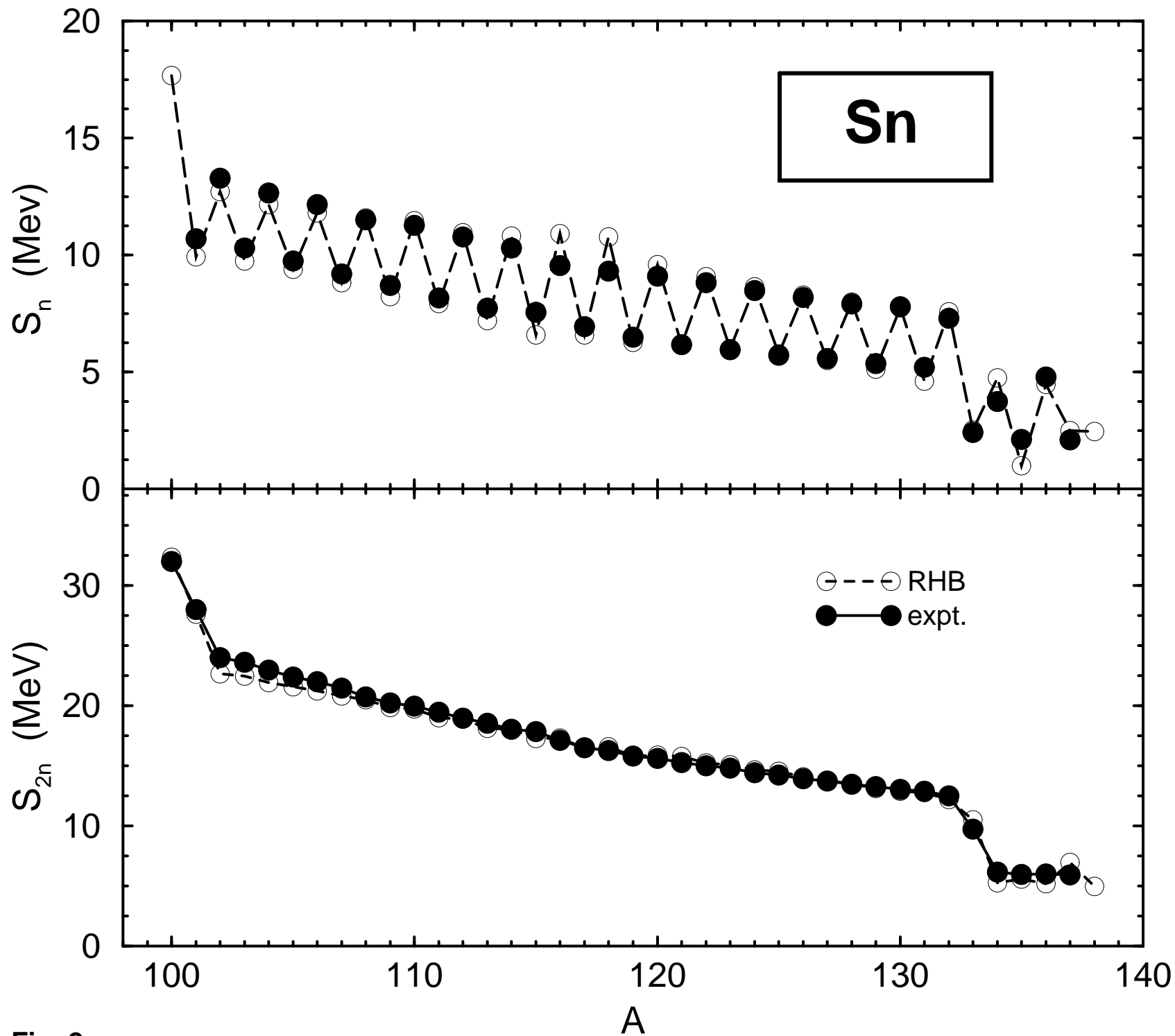


Fig. 2

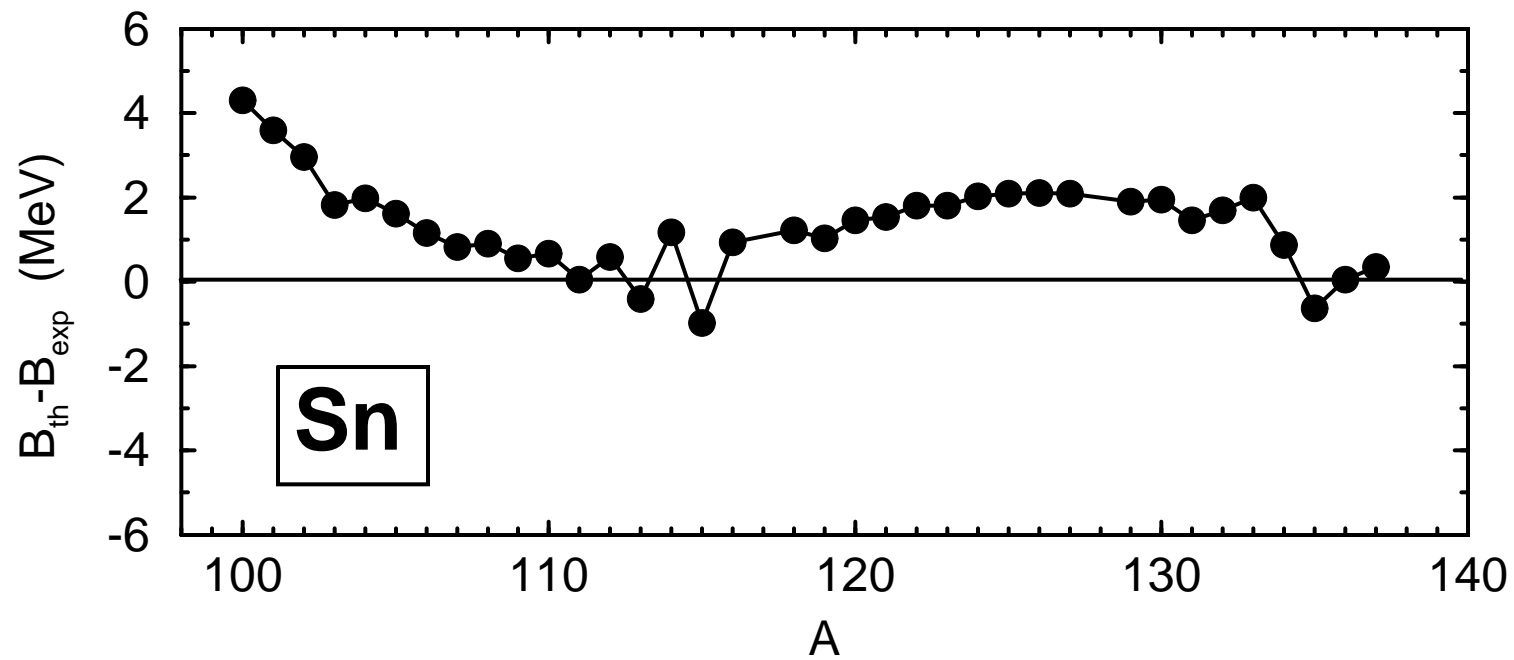
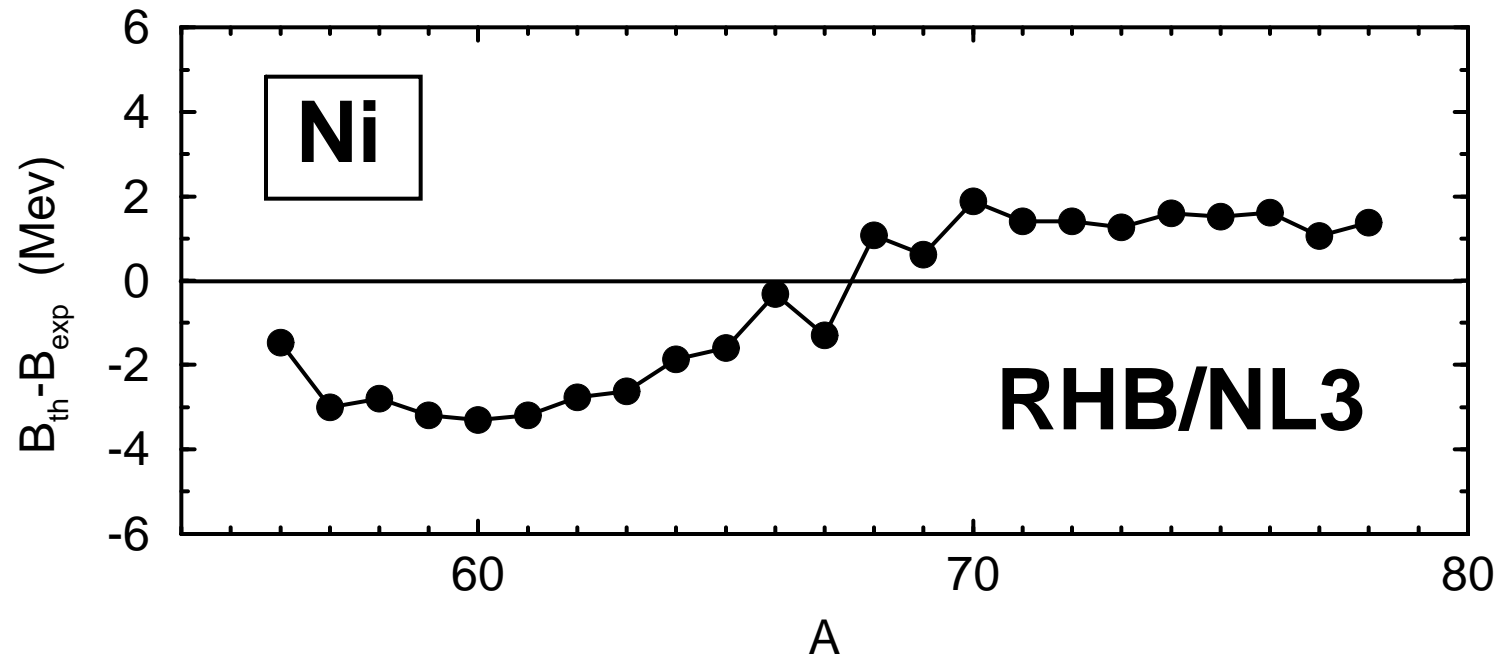


Fig. 3

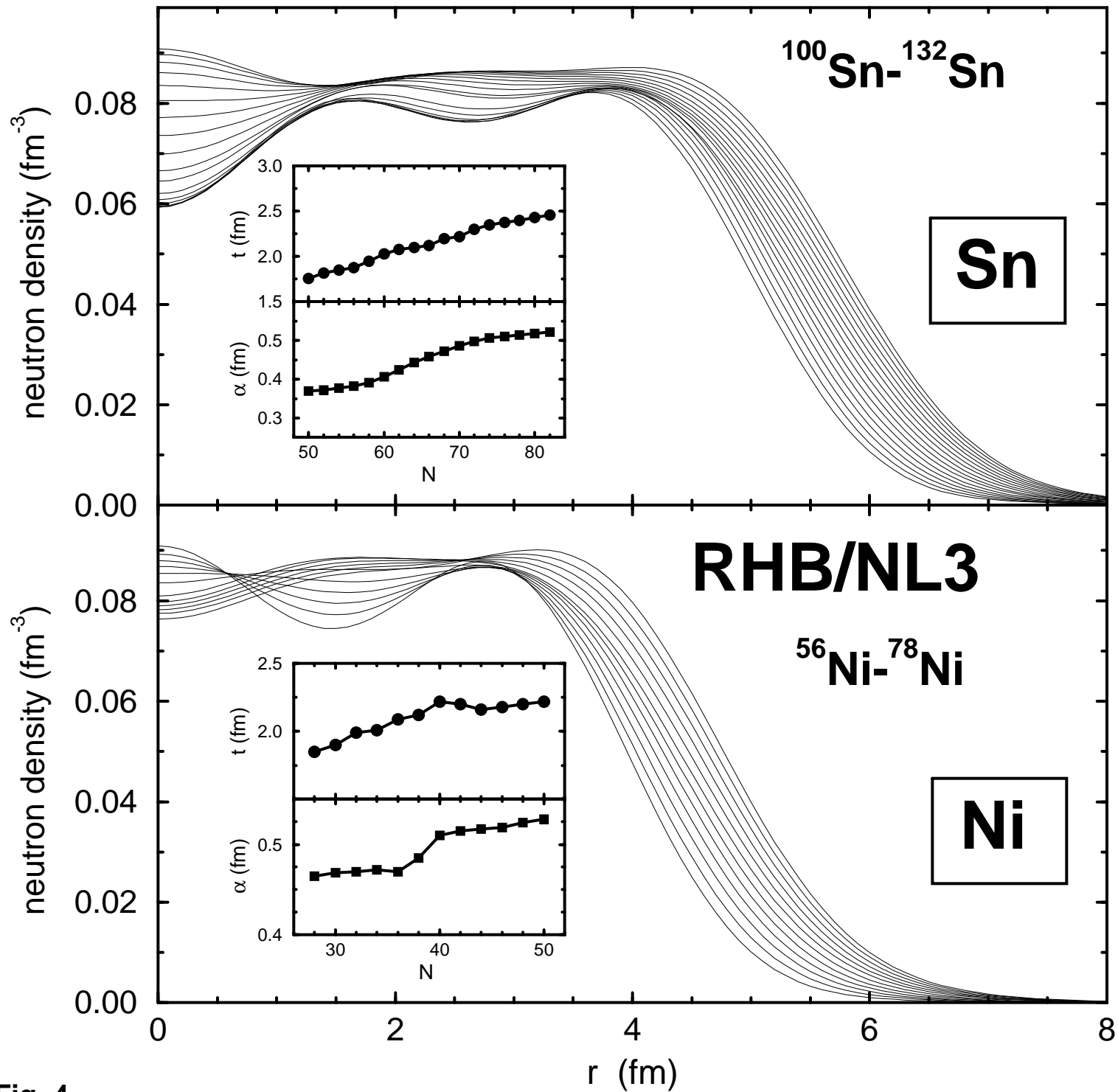


Fig. 4

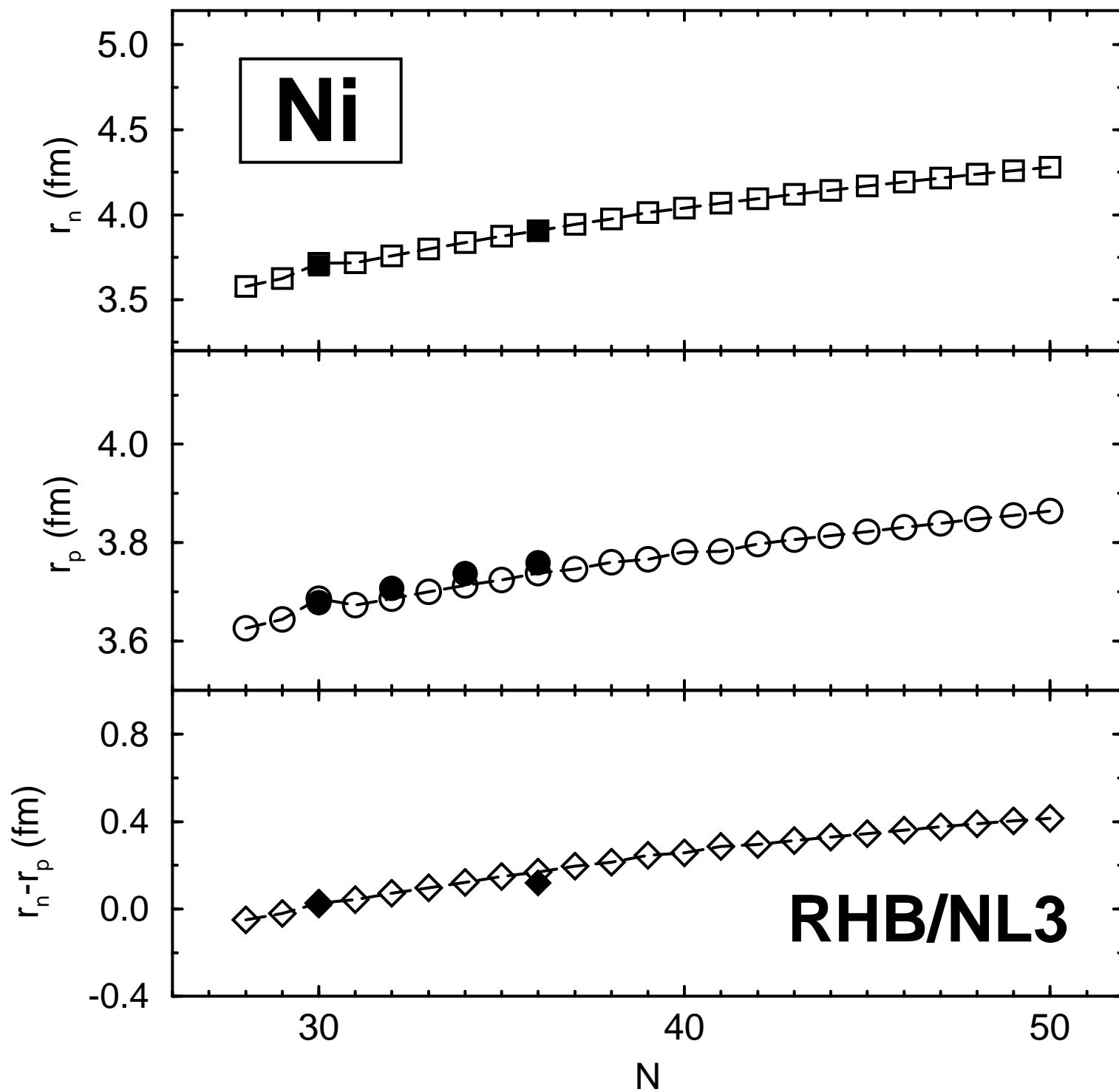


Fig. 5



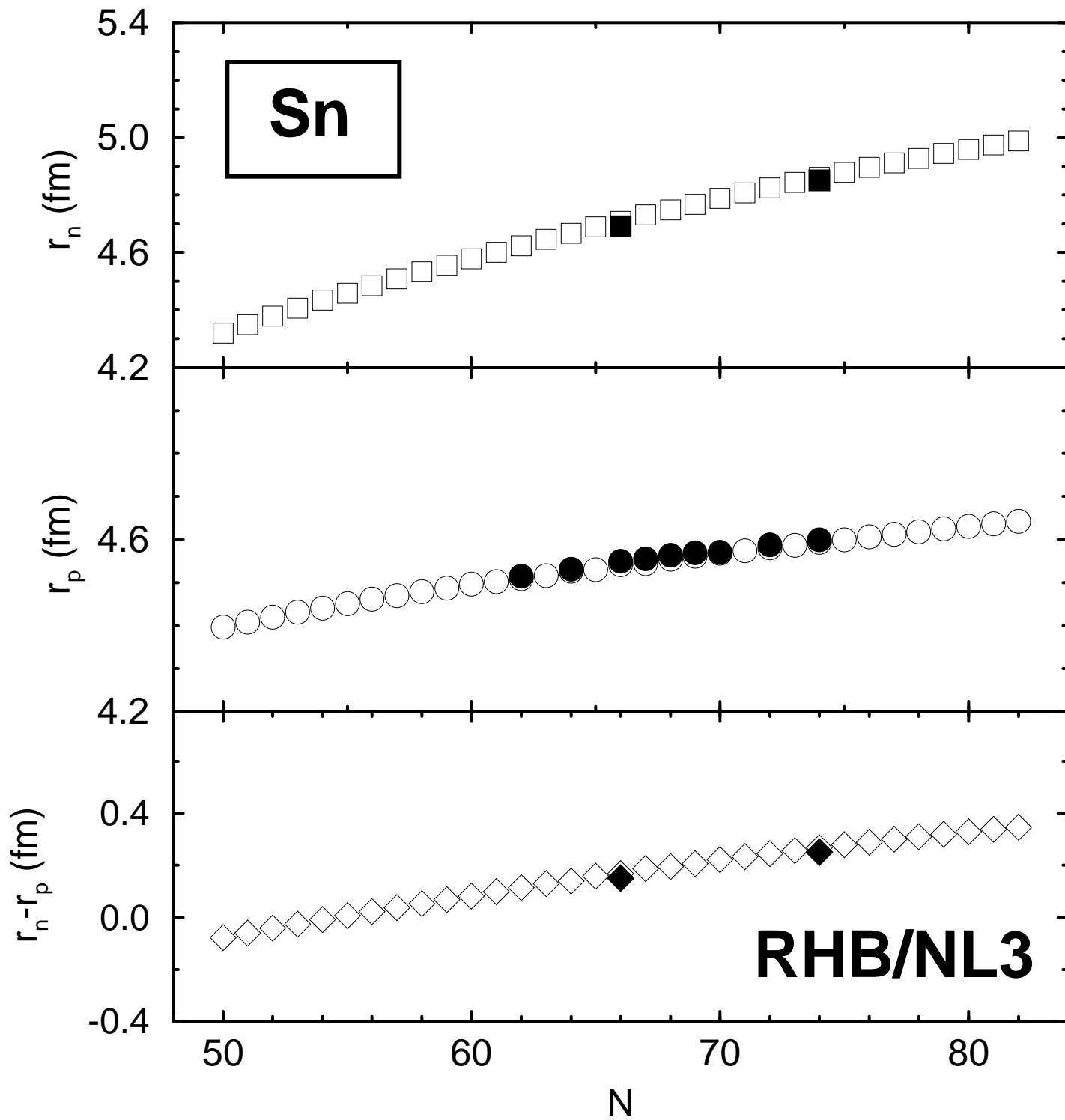


Fig. 6

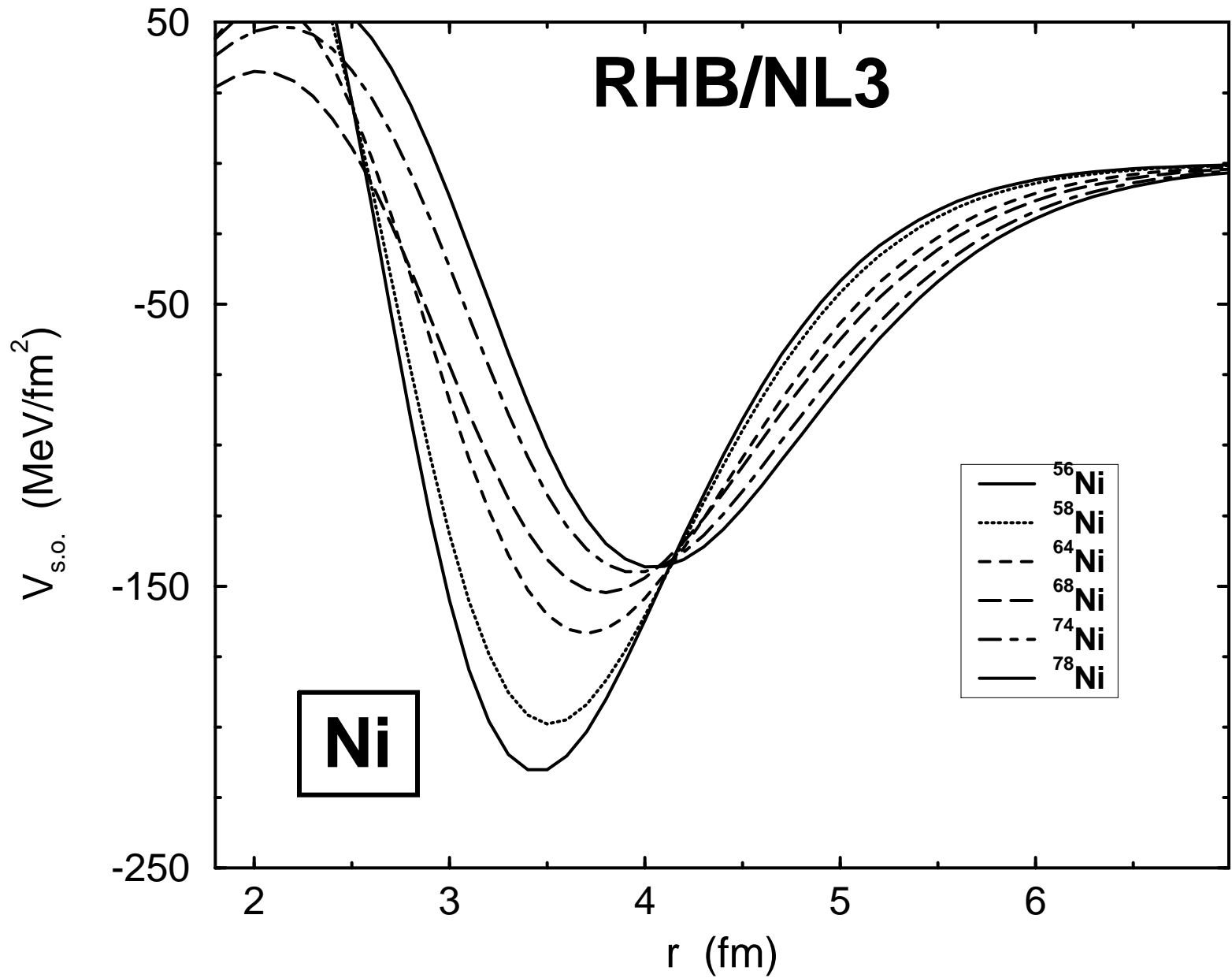
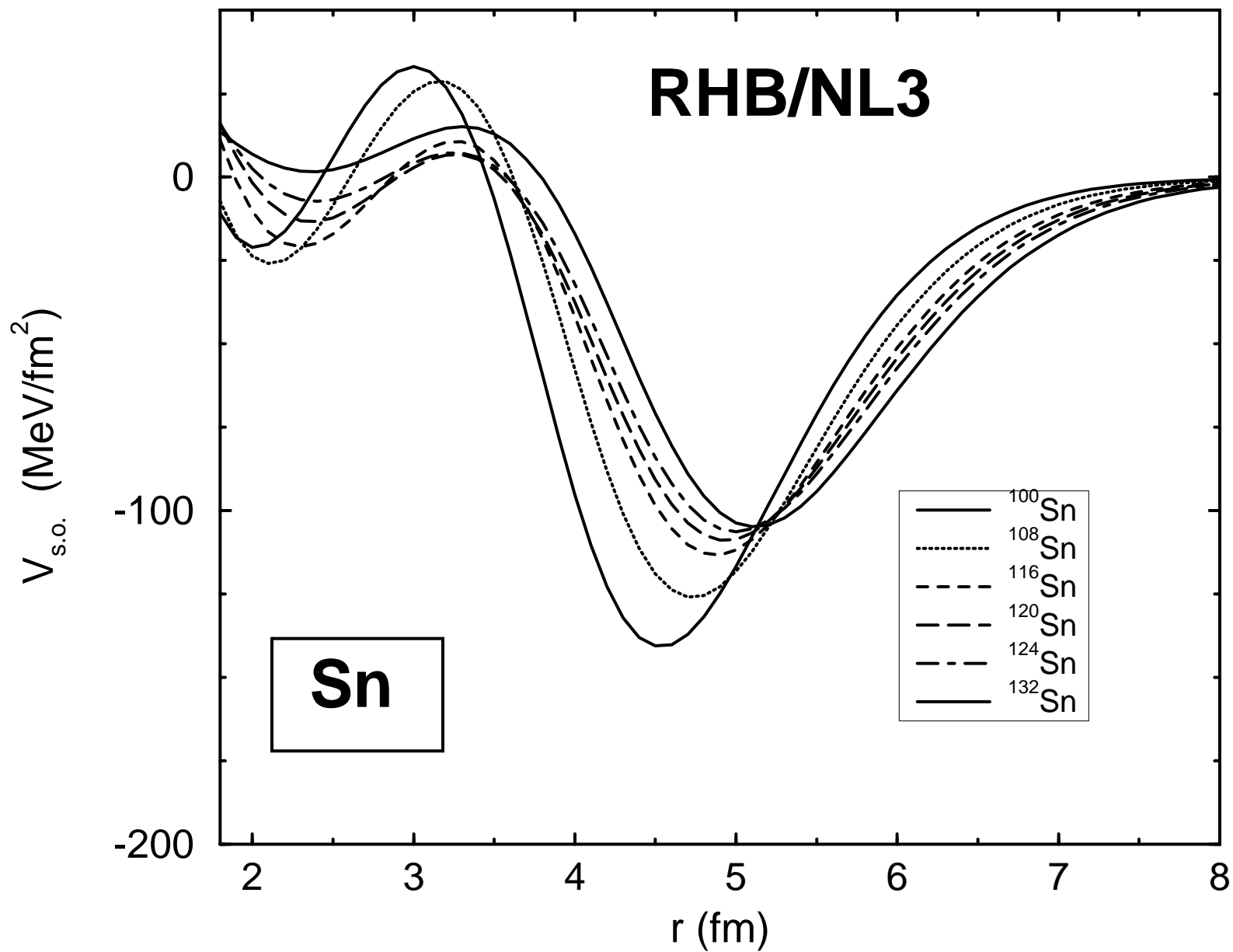


Fig. 7



**Fig. 8**

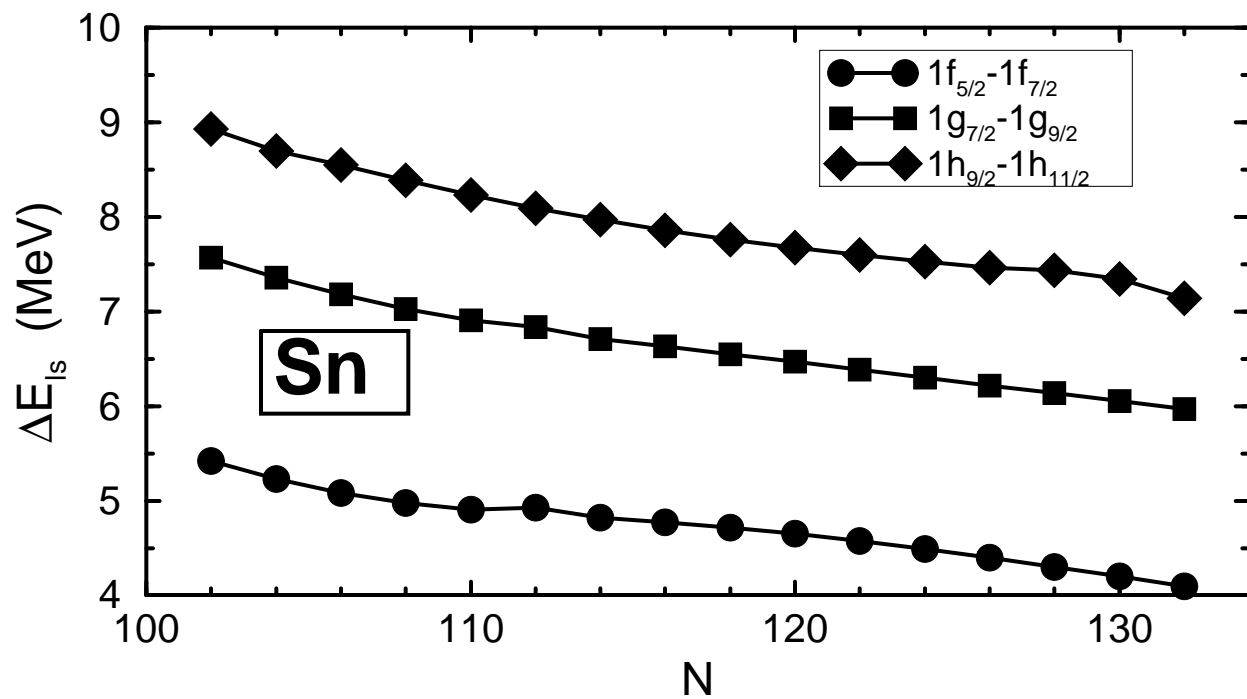
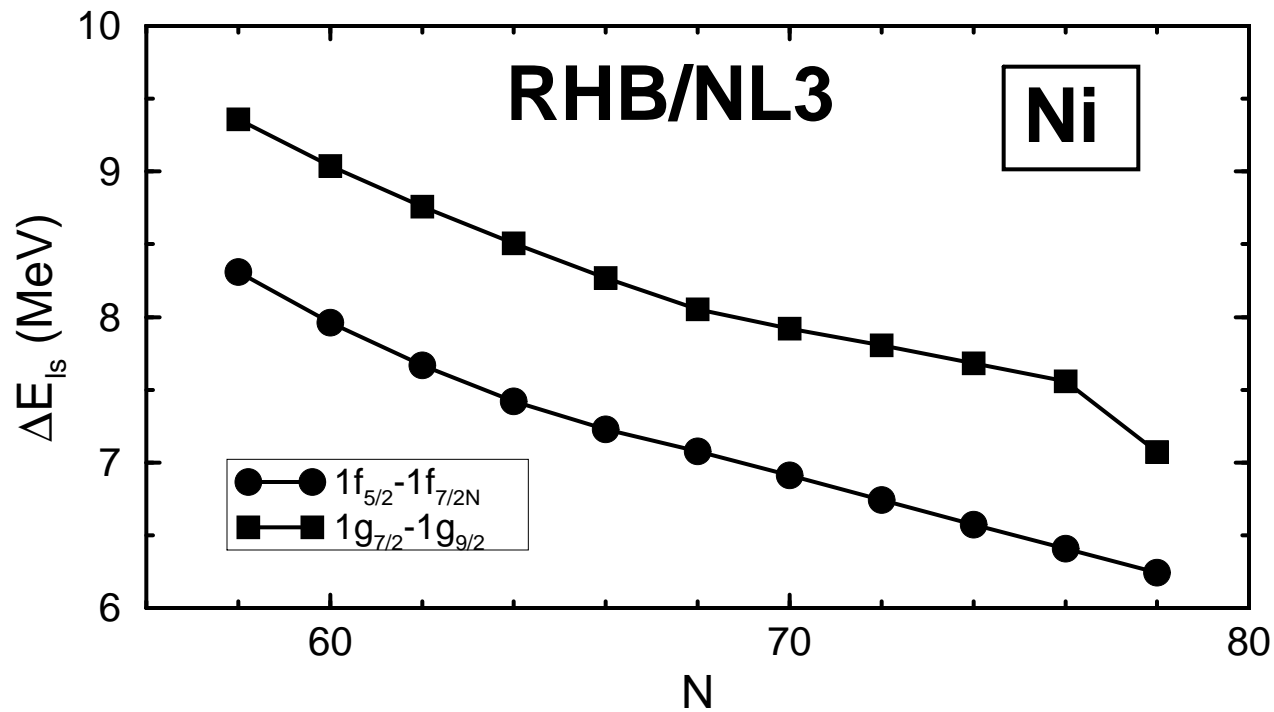


Fig. 9

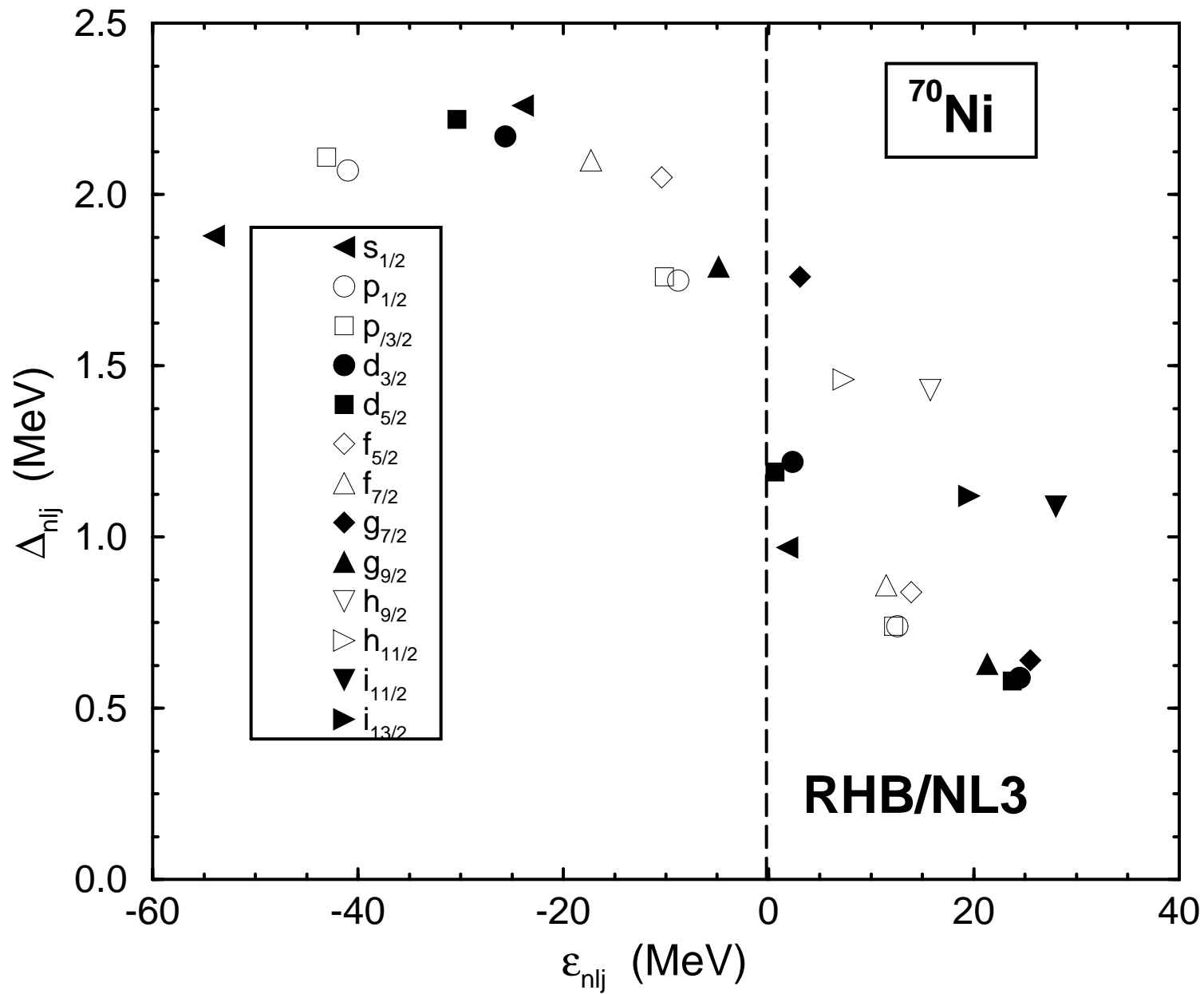


Fig. 10

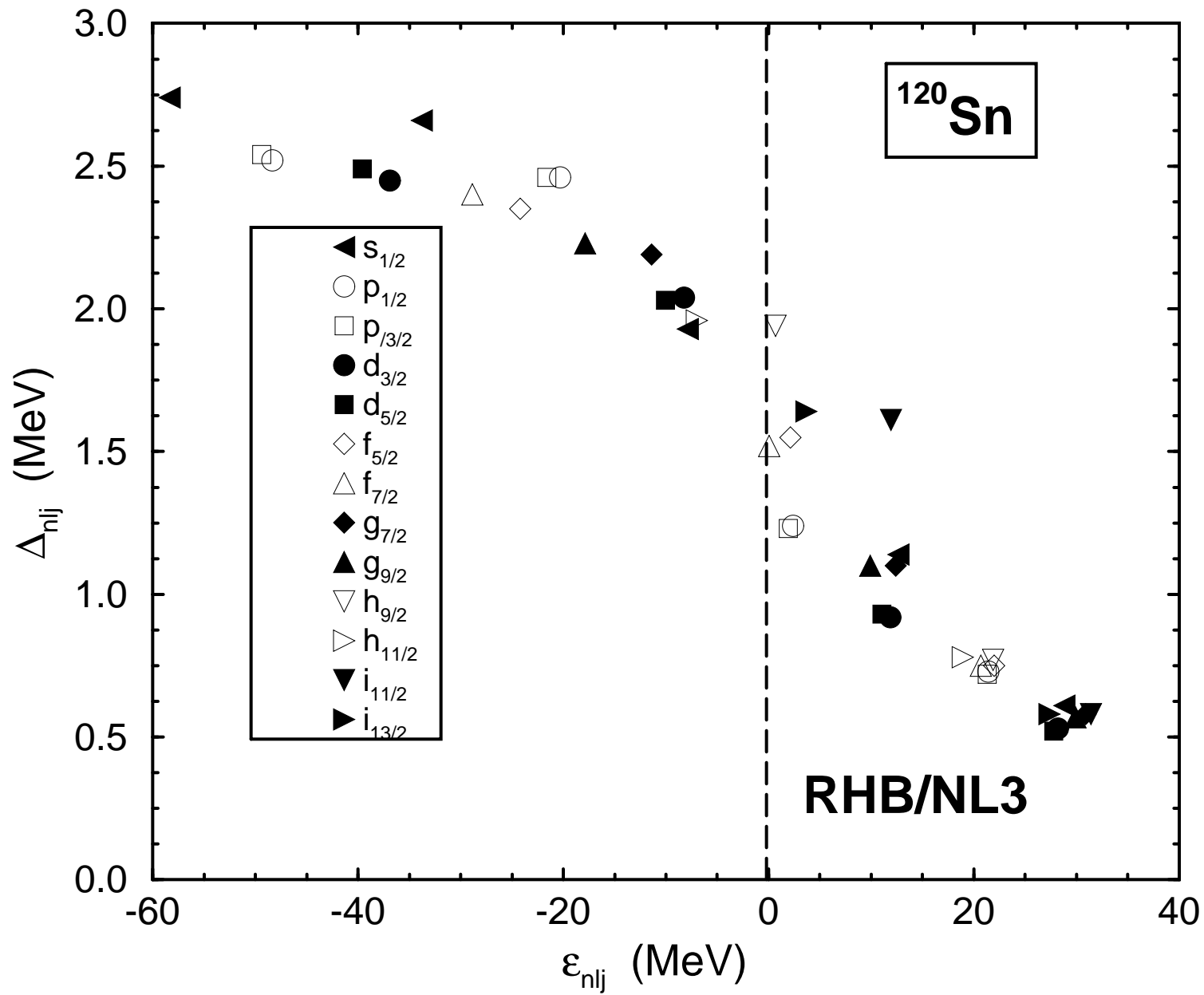


Fig. 11

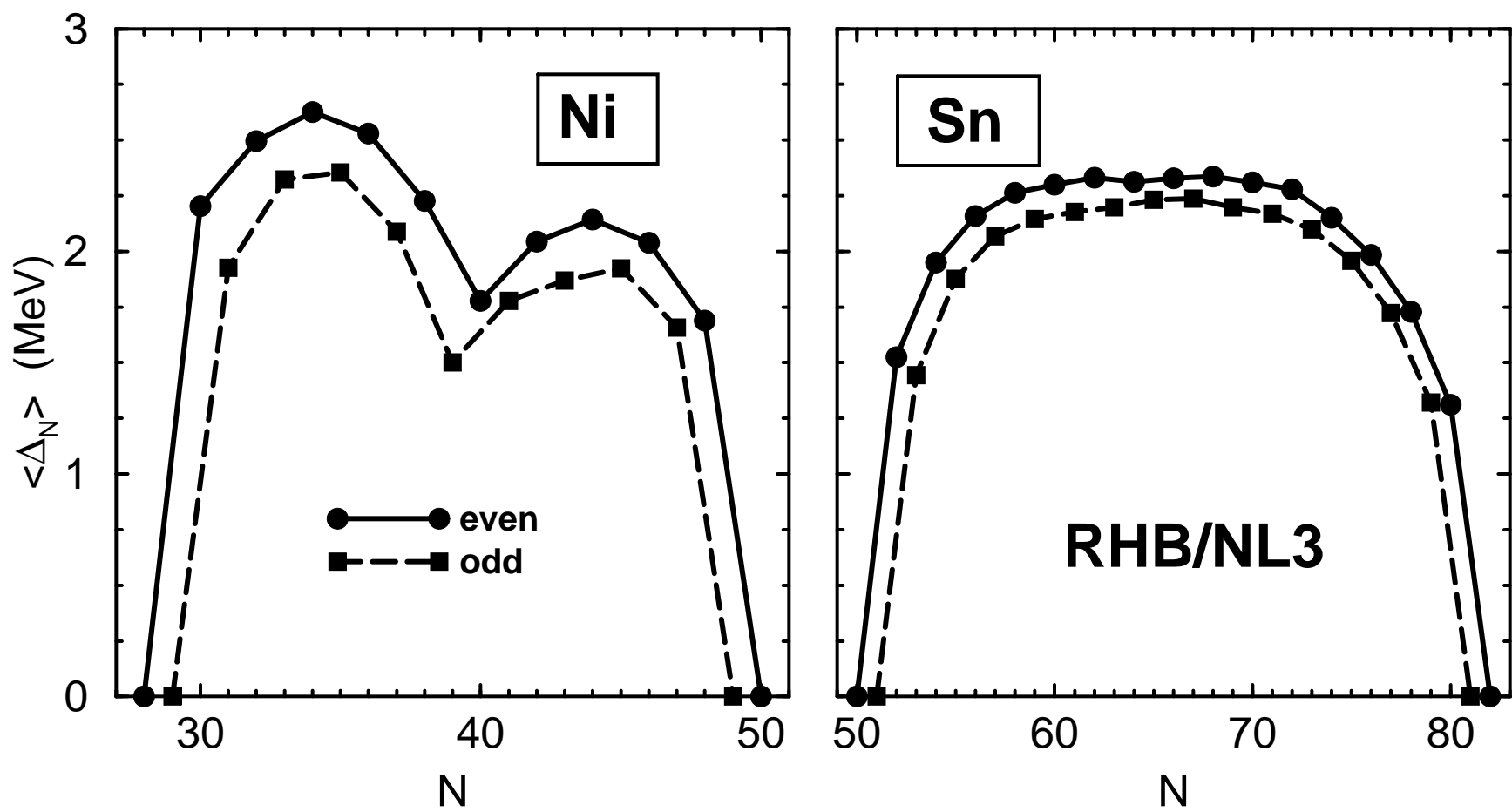


Fig. 12